International Research Journal of Engineering and Technology (IRJET) e-ISSN: 2395-0056
Volume: 08 Issue: 05 | May 2021 www.irjet.net p-ISSN: 2395-0072

Modified DC-DC Boost Converter for Fuel Cell Vehicle Applications

Anjitha Priyan J[1], Dr. Sunila M S[2]

[1]PG Scholar, Dept. of EEE, Govt. Engineering College-Bartonhill, Kerala, India
[2]Associate Professor, Dept. of EEE, Govt. Engineering College-Bartonhill, Kerala, India

---

Abstract - *This paper presents a Modified DC-DC boost converter for fuel cell vehicle application. In fuel cell vehicles, the output voltage of the fuel cell source is typically much lower than the voltage required by the DC bus and also this output voltage drops significantly as the output current increases. In order to match the output voltage of the fuel cell source to the DC bus voltage, a new DC-DC boost converter with a wide input range and high voltage gain was proposed to act as the required power interface, which reduces voltage stress across the power devices and operates with an acceptable conversion efficiency. Also a novel optimization technique for the closed-loop controller design of a boost type DC-DC converter based on the Particle Swarm Optimization (PSO) algorithm is proposed.*

Key Words: **Boost DC-DC converter, Fuel Cell Vehicles, High Voltage-Gain, Wide Input Range, Closed Loop, Particle Swarm Optimisation.**

1. INTRODUCTION

In recent years, the usage of renewable energy systems such as fuel cell and photovoltaic systems are encouraged due to various environmental troubles caused by other fuels, such as climate change and global warming by increased emissions of carbon dioxide. With increasing attention to environmental problems, energy achieved from the fuel cell systems is focused on the low environmental effects and clean energy. Fuel cells are an effective alternative to replace fuels in emergency power systems and vehicles [1]-[3]. Vehicles powered by fuel cell sources may help to reduce transport's dependence on oil, and reduce polluting emissions. However, unlike batteries which have a fairly constant output voltage, the output voltage of fuel cells drops significantly with an increase of output current. Hence, a step-up DC-DC converter with a wide range of voltage-gain is essential to interface between the low voltage fuel-cell source and the high voltage DC bus of the motor drive inverter.

As shown in Fig.1, each energy source might require a specific DC-DC converter to be integrated into the high voltage (HV) DC link of the power-train. For bidirectional electric sources like super capacitors (SCs) and batteries, bidirectional DC-DC converters are essential to absorb the regenerative braking energy, which maximizes the overall efficiency of the system.

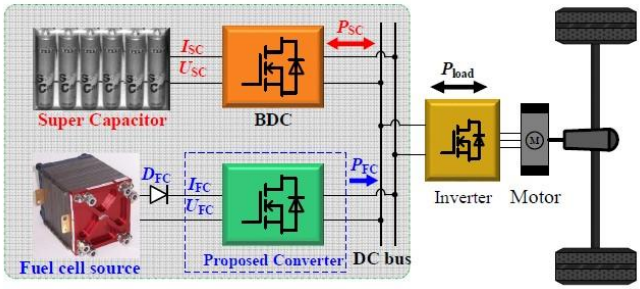

Fig -1: Block diagram of electric vehicle power-train with proposed converter

The proposed DC-DC converter with a high voltage gain is interfaced between low voltage (LV) fuel cell source and HV DC bus. When fuel cell vehicle accelerates, SC stacks supply power from DC bus by bi-directional converter (BDC). When fuel cell vehicle brakes or regenerates, energy is absorbed by SC stacks. When fuel cell vehicle runs smoothly, fuel cell source provides stable energy for inverter by proposed converter with corresponding voltage gain and charges SC stacks if needed. In theory, when the duty cycle approaches unity, the conventional boost converter can achieve a high voltage gain [4]. However, it is difficult to implement a high voltage gain (e.g. more than 6), due to the existence of parasitic elements (stray inductance, capacitance) and the extreme duty cycle required. In addition, the power semiconductors suffer from a high voltage stress - the DC bus voltage.

In order to obtain a DC-DC Boost converter with a high voltage gain and a low voltage stress, many different topologies have been proposed by researchers [5]-[8]. Compared with isolated converters, the cost and magnetic losses of nonisolated converters are lower. A high voltage-gain can be achieved by introducing a coupled inductor to topology e.g. [9]-[10], and the converter can maintain a low device voltage stress. The conventional quadratic DC-DC boost converter in [11] can obtain a high voltage-gain, but the voltage stress across the high side power semiconductors is as high as the output-voltage.

To solve this problem, the switched-capacitor configurations introduced in [12], and [13] are able to obtain a high voltage gain, but they cannot achieve flexible voltage regulation unless they are combined with other DC-DC converters [14]. A topology called the "switched-capacitor-based active-network" (SC-ANC) is presented in [15], the power switches may see a large voltage spike as a result of the leakage inductance of the circuit. The switched-capacitor

circuit was studied in [16]: it achieves flexible voltage regulation by combining it with other DC-DC converters, however the difference in potential between the ground points of the input voltage source side and the load side is a high frequency pulse width modulated (PWM) voltage [17]-[18]. As a result, it may introduce issues associated with du/dt and these may limit its applications [19][20].

The design of the closed loop control parameters is framed as an optimization task such that the PSO algorithm can identify the controller parameters. An appropriate fitness function is then derived for the required objective and is used in the optimization process. The attributes of the large-signal model of the power converter, together with those of the optimization algorithm, provide excellent static and dynamic characteristics at all operating points.

2. PROPOSED SYSTEM

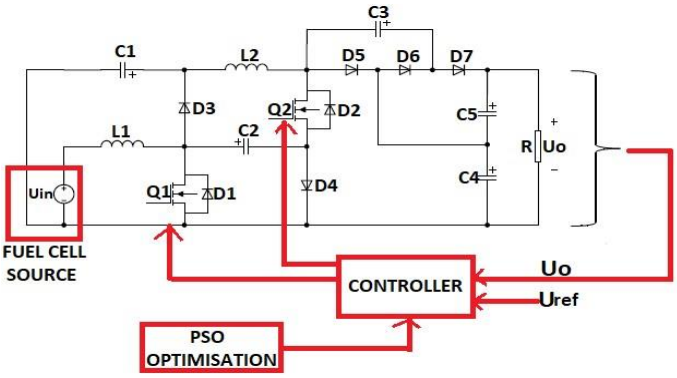

Fig- 2. Configuration of the proposed system

The configuration of the proposed system is shown in Fig.2. In order to boost the output voltage from the fuel cell source, a DC-DC boost converter is used which is having a wide input range, high voltage gain, acceptable conversion efficiency and reduces voltage stress across power devices. But the major drawback of this converter is the varying output voltage when the input from fuel cell source changes significantly. So a voltage source controller can designed in order to achieve suitable static and dynamic performance. And also the closed loop controller parameters are designed by Particle Swarm Optimisation (PSO) technique. Thus the proposed system can act as the required power interface between the fuel cell source and DC bus.

2.1 Configuration of the proposed converter

To address the issues with regard to the conventional converters, a new non-isolated high ratio step-up dc-dc converter is proposed in this paper, which has the following features:

- It reduces the voltage stress across the power devices and has a common ground between the input and output sides.
- The two power switches turn on and off simultaneously. As a result, the control of the converter is simple, and power switches with low on-state resistance can be employed.
- The system operates with a high voltage gain and a wide input voltage range and does not use any extreme values for its duty cycle.

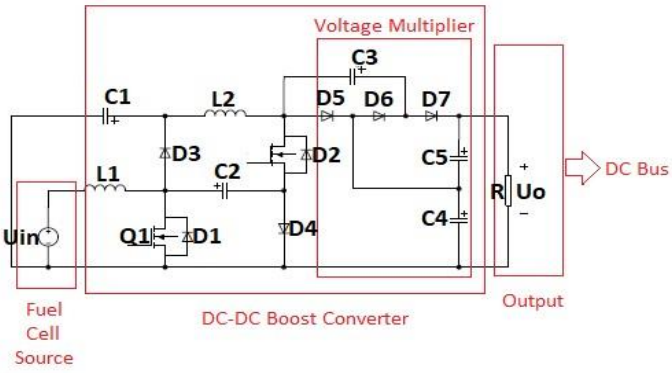

Fig- 3. Proposed DC-DC boost converter topology.

The high voltage gain DC-DC Boost converter is shown in Fig.3. It comprises two active power switches (Q_1 and Q_2), five power diodes (D_3–D_7), two inductors (L_1 and L_2) and five capacitors ($C_1 - C_5$). The fuel-cell source U_in and the inductor L_1 are connected in series to charge capacitors C_1 and C_2 in parallel. Inductor L_2 is another energy storage component which is used to realize a high voltage gain. The ladder type voltage multiplier (capacitors C_3–C_5 and diodes $D_5 - D_7$) can improve the voltage-gain further and reduces the voltage stress across the power semiconductors on the high voltage side.

2.2. Operating principle of the proposed converter

The gate signals of the two power switches (Q_1,Q_2) are identical - (Q_1,Q_2) are turned on and off simultaneously. Therefore, there are two switching states in each switching period, which are shown in Fig.4.

- ***Switching state I***: As shown in Fig.4.(a), Q_1 and Q_2 turn on, L_1 is charged by the DC source U_{in} i.e., ($U_{in}L_1$–Q_1), and L_2 is charged by C_1 and C_2 in series i.e., (C_1–L_2–Q_2–C_2–Q_1). Meanwhile, C_3 is charged by C_2 and C_4 in series i.e., (C_4–D_6–C_3–Q_2–C_2–Q_1).
- ***Switching state II***: As shown in Fig.4.(b), Q_1 and Q_2 turn off, C_1 and C_2 are charged in parallel by the DC source and L_1 i.e., ($U_{in} - L_1 - D_3 - C_1$, and $U_{in} - L_1 - C_2 - D_4$). At the same time, C_4 is charged by the DC source, L_1, and L_2 in series i.e., ($U_{in} - L_1 - D_3 - L_2 - D_5 - C_4$). In addition, C_4 and C_5 are charged by the DC source, L_1, L_2, and C_3 i.e., ($U_{in} - L_1 - D_3 - L_2 - C_3 - D_7 - C_5 - C_4$), as well as through the load R. The output-voltage Uo is equal to the total voltages across C_4 and C_5.

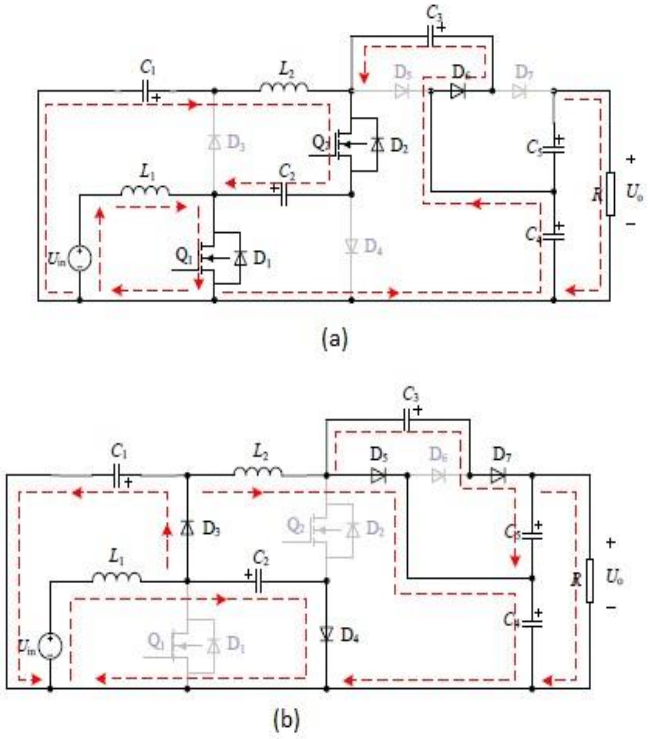

Fig -4: Switching states of the proposed converter (a) Switching state I (b) Switching state II

The comparison of the proposed converter with other existing high voltage gain DC-DC Boost converters is shown in Table 1. It can be seen that the proposed converter achieves a high and wide voltage gain range by increasing the number of diodes by a small amount. Compared with the 3-level DC-DC converter the proposed converter is more suitable for applications requiring a large step-up ratio.

Table -1: Comparisons among the proposed converter and other high voltage gain converters

Topology	DC-DC Boost Converters		
	3-Level	*Transformerless*	*Proposed*
No.of switches	2	2	2
No.of diodes	2	4	5
No.of inductors	2	2	2
No.of capacitors	2	2	2
Voltage-gain	$\frac{1}{(1-d)^2}$	$\frac{4}{(1-d)}$	$\frac{3+d}{(1-d)^2}$
Switch volt stress	dU_0	$U_0/4$	$\frac{(1+d)U_0}{3+d}$
Diode volt stress	U_0	$U_0/2$	$\frac{2U_0}{3+d}$
Common ground	Yes	No	Yes
Efficiency	88%–93%	94%–96%	90%–95%

Considering the selection of the power switches, 3-level DC-DC converter will have its maximum device voltage stress (which is higher than half of the output voltage) when d 6= 0.5, whereas the maximum voltage stress across the power switches is less than half of the output voltage in the proposed converter. Considering the selection of the diodes, the maximum voltage stress across the diodes for the proposed converter is lower than that of the 3-level DC-DC converter. Although the Transformer-less DC-DC Converters has the advantage of the lower voltage stress, it does not have a common ground between the input and the output sides and this may cause additional du/dt issues.

3. STATE SPACE REPRESENTATION OF SYSTEM

It is assumed that the power semiconductors, inductors, and capacitors are analyzed for operation under ideal conditions. The average model and the small-signal model can be obtained by using the state-space averaging method. The capacitances are set such that $C_1 = C_2 = C_3 = C_4 = C_5 = C$ to simplify the analysis. The inductances are defined as L_1 and L_2, the load resistance is R, and $u_{in}(t)$, $u_o(t)$ and d are the input variable, the output variable and the control variable, respectively. $i_{L1}(t)$, $i_{L2}(t)$, $u_{C1}(t)$, $u_{C2}(t)$, $u_{C3}(t)$, $u_{C4}(t)$ and $u_{C5}(t)$ are the state variables. According to Fig. 4(a), C_2, C_3 and C_4 are connected in series in the loop circuit when Q_1 and Q_2 turn on. It means the sum of voltages across C_2, C_3 and C_4 is 0. There is an invalid state variable ($u_{C2}(t) + u_{C3}(t) + u_{C4}(t) = 0$, i.e. there are only two independent variables) in this loop circuit. By including the equivalent series resistance (e.g. $r_1 = r = 0.1\Omega$) in the same loop circuit, the coupling between C_2, $C3$ and C_4 can be removed to avoid the invalid state variable. Similarly, as shown in Fig. 4(b), C_1 and C_2 are connected in parallel when Q_1 and Q_2 turn off, and this means the voltages across C_1 and C_2 should be equal, i.e. there is another invalid state variable. The coupling relationship between C_1 and C_2 can also be removed to avoid the invalid state variable ($u_{C1}(t) + u_{C2}(t) = 0$), by including the equivalent series resistance (e.g. $r_2 = r = 0.1\Omega$) in the loop circuits.

The state space model of system can be represented by following state and output equation respectively.

$$\dot{x} = Ax + Bu$$

$$\dot{y} = Cx + Du$$

3.1. Switching state 1

Switches Q_1 and Q_2 are turned ON:

L_1 is charged by DC source U_{in},

$$\frac{di_{L1}(t)}{dt} = \frac{1}{L_1}U_{in}(t) \quad (1)$$

L_2 is charged by C_1 and C_2 in series,

$$\frac{di_{L2}(t)}{dt} = \frac{1}{L_2}u_{C1}(t) + \frac{1}{L_2}u_{C2}(t) \quad (2)$$

C_2, C_3 ,C_4 are connected in series in loop circuit,

$$u_{C2}(t) + u_{C3}(t) + u_{C4}(t) = 0 \quad (3)$$

So, equivalent series resistance, $r_1 = r = 0.1\Omega$ is included in loop circuit.

$$\frac{di_{L2}(t)}{dt} = -\frac{r}{L_2} i_{L2}(t) + \frac{1}{L_2} u_{C1}(t) + \frac{1}{L_2} u_{C2}(t) \quad (4)$$

Current through capacitor C_1 is,

$$\frac{du_{C1}(t)}{dt} = \frac{-1}{C_1} i_{L2}(t) \quad (5)$$

Current through capacitor C_2 is,

$$\frac{du_{c2}(t)}{dt} = \frac{-1}{C} i_{L2}(t) - \frac{1}{C_r} u_{C2}(t) + \frac{1}{C_r} u_{C3}(t) - \frac{1}{C_r} u_{C4}(t) \quad (6)$$

Capacitor C_3 is charged by C_2 and C_4 in series,

$$\frac{du_{C3}(t)}{dt} = \frac{1}{C_r} u_{C2}(t) - \frac{1}{C_r} u_{C3}(t) + \frac{1}{C_r} u_{C4}(t) \quad (7)$$

Current through capacitor C_4 is,

$$\frac{du_{c4}(t)}{dt} = \frac{-1}{C_r} u_{C2}(t) + \frac{1}{C_r} u_{C3}(t) - \frac{R+r}{CR_r} u_{C4}(t) - \frac{1}{C_R} u_{C5}(t) \quad (8)$$

Current through capacitor C_5 is,

$$\frac{du_{C5}(t)}{dt} = -\frac{1}{CR} u_{C4}(t) - \frac{1}{CR} u_{C5}(t) \quad (9)$$

The output voltage across R is the sum of total voltage across C_4 and C_5,

$$u_0(t) = u_{C4}(t) + u_{C5}(t) \quad (10)$$

3.2. Switching state 2

Switches Q_1 and Q_2 are turned OFF:

Capacitors C_1 and C_2 are charged in parallel by DC source and L_1,

$$\frac{di_{L1}(t)}{dt} = -\frac{1}{L_1} u_{c2}(t) + \frac{1}{L_1} U_{in}(t) \quad (11)$$

Capacitors C_4 is charged by the DC source and L_1 and L_2 in series,

$$\frac{di_{L2}(t)}{dt} = -\frac{1}{L_2} u_{c2}(t) - \frac{1}{L_2} u_{C4}(t) \quad (12)$$

C_1, C_2 are connected in parallel when Q_1 and Q_2 are turned OFF,

$$u_{C1}(t) + u_{C2}(t) = 0 \quad (13)$$

So, equivalent series resistance, $r_1 = r = 0.1\Omega$ is included in loop circuit.

Current through capacitor C_1 is,

$$\frac{du_{C1}(t)}{dt} = \frac{-1}{C_r} u_{C1}(t) + \frac{1}{C_r} u_{C2}(t) \quad (14)$$

Current through capacitor C_2 is,

$$\frac{du_{c2}(t)}{dt} = \frac{1}{C} i_{L1}(t) - \frac{1}{C} i_{L2}(t) + \frac{1}{C_r} u_{C1}(t) - \frac{1}{C_r} u_{C2}(t) \quad (15)$$

Capacitor C_4 and C_5 is charged by DC source, L_1, L_2 and C_3,

$$\frac{du_{C3}(t)}{dt} = \frac{-1}{C_r} u_{C3}(t) + \frac{1}{C_r} u_{C5}(t) \quad (16)$$

Current through capacitor C_4 is,

$$\frac{du_{c4}(t)}{dt} = \frac{1}{C} i_{L2}(t) - \frac{1}{C_R} u_{C4}(t) - \frac{1}{CR_r} u_{C5}(t) \quad (17)$$

Current through capacitor C_5 is,

$$\frac{du_{C5}(t)}{dt} = -\frac{1}{Cr} u_{C3}(t) - \frac{1}{CR} u_{C4}(t) - \frac{R+r}{CR_r} u_{C5}(t) \quad (18)$$

The output voltage across R is the sum of total voltage across C_4 and C_5,

$$u_0(t) = u_{C4}(t) + u_{C5}(t) \quad (19)$$

When S=1, the ON-state period is $d \times T$ and when S=0, the OFF-state period is (1-d)T.

The above equations can be represented as state space model as shown below in eq(20).

Choosing the state variables as, $i_{L1} = x_1$, $i_{L2} = x_2$, $u_{C1} = x3$, $uC2 = x4$, $uC3 = x5$, $uC4 = x6$, $uC5 = x7$, $Uin(t) = u$, $U_o(t) = Y$;

$$\begin{bmatrix} \hat{x_1} \\ \hat{x_2} \\ \hat{x_3} \\ \hat{x_4} \\ \hat{x_5} \\ \hat{x_6} \\ \hat{x_7} \end{bmatrix} = \begin{bmatrix} 0 & 0 & 0 & \frac{d-1}{L_1} & 0 & 0 & 0 \\ 0 & \frac{-rd}{L_2} & \frac{d}{L_2} & \frac{1}{L_2} & 0 & \frac{d-1}{L2} & 0 \\ 0 & \frac{-d}{C} & \frac{d-1}{C_r} & \frac{1-d}{C_r} & 0 & 0 & 0 \\ \frac{1-d}{C} & \frac{-1}{C} & \frac{1-d}{C_r} & \frac{1}{C_r} & \frac{d}{C_r} & \frac{d}{C_r} & 0 \\ 0 & 0 & 0 & \frac{d}{C_r} & \frac{-1}{C_r} & \frac{d}{C_r} & \frac{1-d}{C_r} \\ 0 & \frac{1-d}{C} & 0 & \frac{d}{C_r} & \frac{-1}{CR} - \frac{d}{C_r} & \frac{-1}{CR} & \frac{-1}{CR} \\ 0 & 0 & 0 & 0 & \frac{1-d}{C_r} & \frac{-1}{CR} & \frac{d}{C_r} - \frac{R+r}{CR_r} \end{bmatrix} \begin{bmatrix} x_1 \\ x_2 \\ x_3 \\ x_4 \\ x_5 \\ x_6 \\ x_7 \end{bmatrix} + \begin{bmatrix} \frac{1}{L_1} \\ 0 \\ 0 \\ 0 \\ 0 \\ 0 \\ 0 \end{bmatrix} u$$

$$Y = \begin{bmatrix} 0 & 0 & 0 & 0 & 0 & 1 & 1 \end{bmatrix} \begin{bmatrix} x_1 \\ x_2 \\ x_3 \\ x_4 \\ x_5 \\ x_6 \\ x_7 \end{bmatrix} \quad (20)$$

4. STEADY-STATE VOLTAGE GAIN ANALYSIS

If the switching period for the power switches is T, then, dT is the on-state period, and (1-d) T is the off-state period, where d is the duty cycle of the power switches. It is assumed that the capacitor voltage and the inductor current are constant during each switching period, and the forward voltage drop and the on-state resistance of the power semiconductors are ignored. According to the volt-second balance principle for inductors L_1 and L_2:

$$\begin{cases} U_{in} \times dT + (U_{in} - U_{C2}) \times (1-d)T = 0 \\ (U_{C1} + U_{C2}) \times dT + (U_{C2} - U_{C4}) \times (1-d)T = 0 \end{cases} \quad (21)$$

The voltage relationship between the output and capacitor voltages can be found, in terms of the two switching states which are shown in Fig.4:

$$\begin{cases} U_{C1} = U_{C2} \\ U_{C3} = U_{C5} = U_{C2} + U_{C4} \\ U_0 = U_{C4} + U_{C5} \end{cases} \quad (22)$$

As a result, the output voltage Uo can be obtained from (21) and (22) as follows:

$$U_0 = \frac{3+d}{(1-d)^2} \times U_{in} = M \times U_{in} \quad (23)$$

where M is the conversion ratio, i.e. the voltage gain. (23) shows that the proposed converter can theoretically obtain a high and wide voltage gain range.

5. PARAMETER DESIGN

5.1 Design of the power switches and diodes

The design of the power switches and diodes should refer to the most severe conditions that the semiconductor devices will operate in. Assuming that the maximum required voltage gain is 10 and the load power is 400W, the duty cycle d and the output current I_o can be obtained as follows:

$$\begin{cases} d = 0.3 \\ U_0 = 400V \\ I_0 = 1A \end{cases} \quad (24)$$

It can be deduced that the maximum mean voltage stresses across Q_1 and Q_2 are 70V and 166V respectively, and the maximum mean current stresses on Q_1 and Q_2 are 16.5A and 6.2A respectively. Similarly, it can be derived that the maximum mean voltage stress across D_3 and D_4 is 70V, which is equal to that of Q_1. In addition, the maximum mean current stress on D_3 and D_4 is 5.8A, and the maximum mean voltage and current stresses on D_5 – D_7 are 234V and 1.9A, respectively.

5.2. Design of the inductors and capacitors

Assuming that the maximum required current ripple in the inductors is ΔI_L, the inductances can be calculated when L is in the charging state as given in (25):

$$L = u_L \frac{dt}{di_L} \quad (25)$$

where,

$di_L = \Delta I_L$ and $dt = \frac{d}{f_s}$.

The inductances of L_1 and L_2 can be derived as (26):

$$\begin{cases} L_1 = \frac{d \times U_{in}}{\Delta I_{L1} \times f_s} \\ L_2 = \frac{4d \times U_{in}}{(1-d)^2 \times \Delta I_{L2} \times f_s} \end{cases} \quad (26)$$

Assuming that the maximum acceptable voltage ripple across the capacitor is ΔU_C, the capacitances can be calculated as (27):

$$C = i_C \frac{dt}{du_c} \quad (27)$$

where,

$du_C = \Delta U_C$ and $dt = \frac{d}{f_s}$

The capacitances of the five capacitors can be calculated as (28):

$$\begin{cases} C_1 = \frac{2d \times I_0}{(1-d) \times \Delta U_{C1} \times f_s} \\ C_2 = \frac{(1+d) \times I_0}{(1-d) \times \Delta U_{C2} \times f_s} \\ C_3 = \frac{I_0}{\Delta U_{C3} \times f_s} \\ C_4 = \frac{(1+d) \times I_0}{\Delta U_{C4} \times f_s} \\ C_5 = \frac{d \times I_0}{\Delta U_{C5} \times f_s} \end{cases} \quad (28)$$

6. RESULTS AND DISCUSSION

The parameters of the experimental converter are listed in Table 2. An adjustable dc source with a range of $U_{in} = 40V$ – $120V$ is used to emulate the fuel cell stack source. Hybrid power switches (MOSFETs, IRFP250N and IXTH88N30P) are employed in the low and the high voltage sides, respectively. DSEC60-03A diodes are used on the low voltage side and DPF60IM400HB diodes are used on the high voltage side.

Table -2: Simulation Parameters

Parameter	Symbol	Specification
Input Voltage	Uin	20-80V
Output Voltage	Uo	400V
Rated Power	P	300W
Switching frequency	fs	20kHz
Inductor	L1	330μH
Inductor	L2	1mH
Electrolytic Capacitor	C1/C2	540μF
Film Capacitor	C3/C5	20μF
Film Capacitor	C4	40μF
Power Switch	Q1	IRFP250N
Power Switch	Q2	IXTH88N30P
Diode	D3/D4	DSEC60-03A
Diode	D5/D6/D7	DPF60IM400HB

In addition, the switching frequency is 20 kHz, the inductors are L_1 = 330μH and L_2=1mH respectively (the inductances are increased to keep the current continuous), the electrolytic capacitances are $C_1 = C_2 = 540\mu F$, and the film capacitances are $C_3 = C_5 = 20\mu F$, $C_4 = 40\mu F$. The input voltage U_{in} is variable from 40V to 80V, the reference output voltage

is 400V, and the load resistance is R = 533Ω (i.e. the rated power=300W).

6.1. Open Loop System

A pulse generator is used to give the required switching pulse shown in Fig.5. with a duty cycle of d=0.3. Simulation results of the open loop system is shown in Fig.6. When an input voltage of 60V DC is applied, an output voltage of 400V DC is obtained.

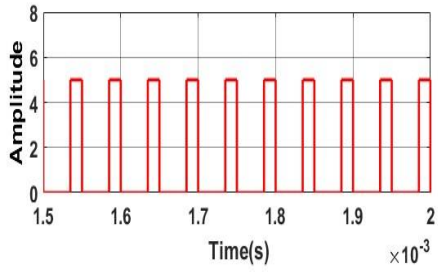

Fig -5: Switching Pulse

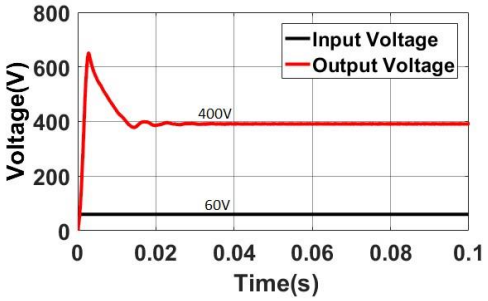

Fig -6: Input & Output Voltage Waveform

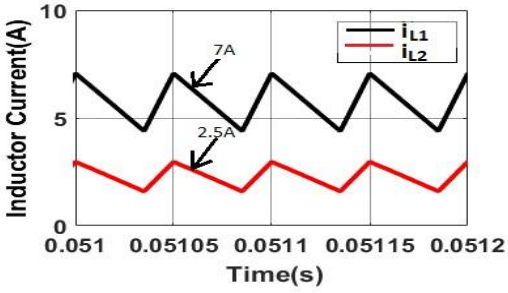

Fig -7: Current through inductor L_1 and L_2

The inductor current i_{L1} and i_{L2} in the steady state are shown in Fig.7, when $U_{in} = 60V$, and $U_o = 400V$. From Fig.7, it is clear that i_{L1} increases linearly when switch is closed. When switch is open, i_{L1} decreases linearly. The average value of i_{L1} is about 7A while the ripple rate is about 12.5%. Similarly, Fig.7. shows that the inductor current i_{L2} has the same trend as i_{L1} i.e., the average value of i_{L2} is approximately 2.5A.

6.2. Closed Loop System

In the closed-loop control system, first, the actual output voltage U_0 is compared with its reference voltage using a comparator and the error voltage, so obtained, is processed by the PI controller. The output voltage of the PI controller is an analog signal which must be converted into a gating pulse for the MOSFET with an adjustable duty cycle. This task is performed by the modulator, which compares the PI controller output voltage with a ramp signal so that the output of the modulator is a gating pulse with its duty cycle varying in accordance with PI controller output voltage.

Closed loop results of input and output voltage of the system are shown in Fig.8. Input voltage is varied at a range of 20V, 30V and 40V and an output voltage of 400V DC is obtained.

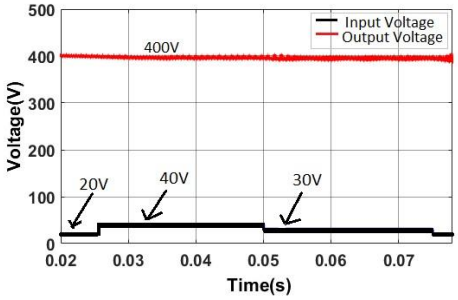

Fig -8: Closed loop input and output voltage waveform

6.3. Fuel Cell Stack Implementation

The fuel cell stack is the heart of a fuel cell power system. It generates electricity in the form of direct current (DC) from electro-chemical reactions that take place in the fuel cell. A single fuel cell produces less than 1 V, which is insufficient for most applications. Therefore, individual fuel cells are typically combined in series into a fuel cell stack. A typical fuel cell stack may consist of hundreds of fuel cells.

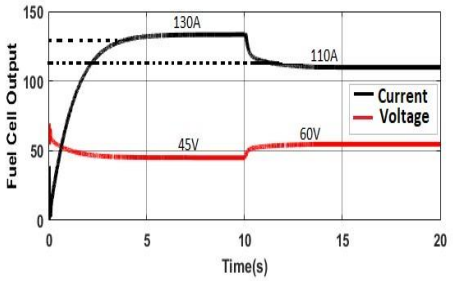

Fig -9: Output voltage and output current waveform of fuel cell stack

The output voltage and output current waveform of fuel cell stack with an output voltage of 60V is shown in Fig.9. Both voltage and current changes its value due to transient state. Voltage decreases initially and remains constant after 10s whereas current increases and remains contant after 10s.

The fuel cell stack parameter variations are shown in Fig.10. From 0 to 10s, flow rate starts increasing and remains constant until it reaches 50lpm. After 10s, flow rate increases upto 90lpm. The voltage and current required for the system are controlled by changing the flow rate of hydrogen and oxygen. As the flow rate is increased, there can be a reduction in utilisation of hydrogen from 100% to 42%. Whereas oxygen utilisation remains constant at 60%. Also upto 10s, oxygen and hydrogen consumption gradually increases and remains constant. After 10s, its consumption decreases and remains constant. At time, t=0, due to transient state, stack efficiency first increase and then decreases and remains constant. With constant stack consumption, stack efficiency again decreases and remains constant after 10s.

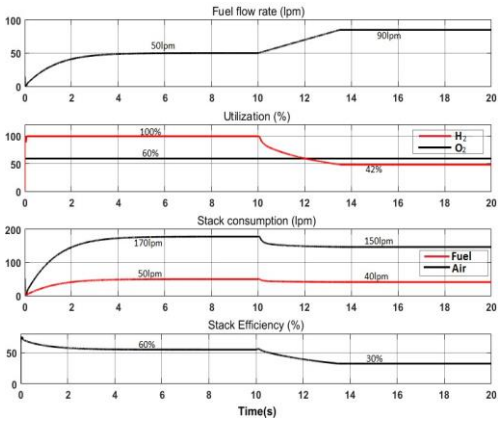

Fig -10: Output voltage waveform of fuel cell stack

7. PARTICLE SWARM OPTIMISATION

The design of the closed loop control parameters framed as an optimization task such that the PSO algorithm can identify the controller parameters. An appropriate fitness function is then derived for the required objective and is used in the optimization process. The attributes of the large-signal model of the power converter, together with those of the optimization algorithm, provide excellent static and dynamic characteristics at all operating points.

Particle swarm optimization (PSO) is a population-based, robust, stochastic optimization technique developed in 1995 by Eberhart and Kennedy, and is inspired by social behavior of fish schooling or bird flocking. PSO is initialized with a number of random agents (particles) that constitute a swarm moving in the search space looking for optima by updating the particles positions during the generations. Each particle represents a candidate solution to the problem at hand. In a PSO system, particles change their positions by flying around in a multi-dimensional search space until a relatively unchanging position has been encountered, or until computational limitations are exceeded.

Boost type DC-DC converters are non-linear systems, and output voltage regulation in these converters using a traditionally derived feedback controller does not yield good dynamic responses at different operating points over the complete operating range. This novel optimization method can be designed to yield a robust, closed loop controller structure with stable static and dynamic characteristics for operating points over the whole operational range of the converter.

In the PSO algorithm shown in Fig.11., the population has n particles and each particle is an m-dimensional vector, where m is the number of optimized parameters. Incorporating the above modifications, the computational flow of PSO technique can be described in the following steps:

- Step 1: Initialize parameters.
- Step 2: Initialize population.
- Step 3: Evaluate fitness value.
- Step 4: Find particle best.
- Step 5: Find global best.
- Step 6: Update velocity.
- Step 7: Update position.
- Step 8: Evaluate.
- Step 9: Repeat steps 4 to 8 until a stopping criteria is met.

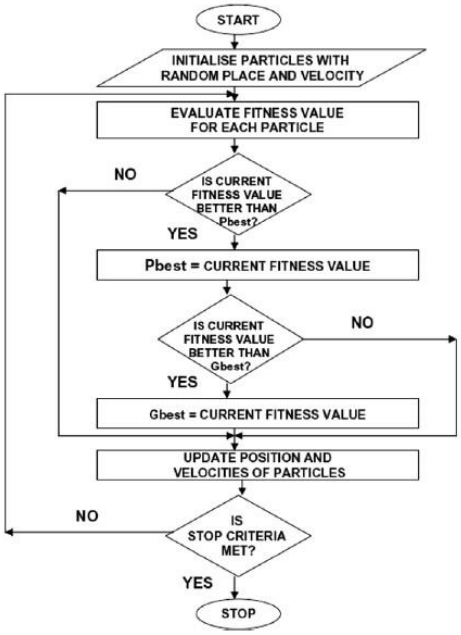

Fig -11:PSO Algorithm

7.1. PSO Results

In a PSO system, particles change their positions by flying around a multi-dimensional search space until a relatively unchanging position has been encountered. Fig.12. shows a swarm with n=100, initialised randomly in the entire search space. Swarm is called the cluster of moving particles and 'n' is the number of particles.

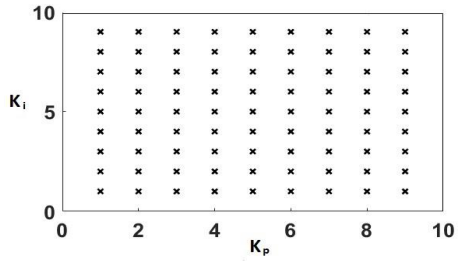

Fig -12: Swarm with n=100, initialized randomly in the entire search space

Evolution of the best values for controller parameters K_p and K_i are shown in Fig.13. The entire particles moves along the entire search space until it has attained the best value for

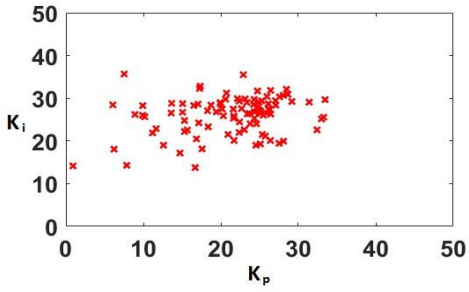

Fig -13: Evolution of the best values for K_p and K_i

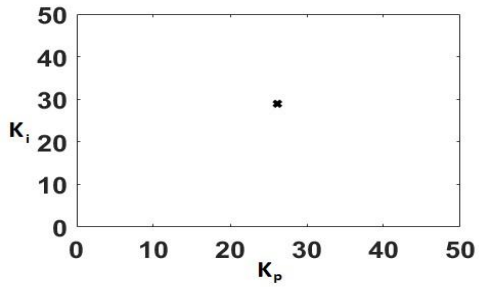

Fig -14: Best values of K_p and K_i

K_p and K_i. The best position of K_p and K_i is obtained as shown in Fig.14. and the controller constants obtained through standard PSO are: K_p = 27 and K_i = 28.

7.2. Overall System with Particle Swarm Optimisation

Configuration of overall DC-DC boost converter with PSO consists of input from the fuel cell source, PSO based PI controller and DC-DC boost converter and the output section. Output voltage of overall system is shown in Fig.15. where the input from fuel cell source of 20V to 60V is varied and an output voltage of 400V DC with better response is obtained.

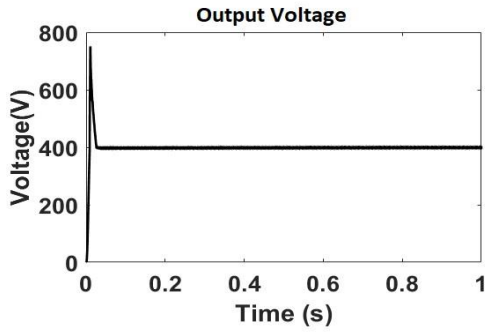

Fig -15: Simulation results of the overall system with PSO

8. PERFORMANCE COMPARISON OF PI CONTROLLER WITH PSO AND ZEIGLER NICHOL'S OPTIMISATION

Fig.16. shows the step response of the system with Zeigler Nichol's Optimisation. From the figure the values for K=0.33, L=0.2 and T=1.6-L. According to Zeigler Nichol's (ZN) Optimisation,

$$T_i = \frac{L}{0.3} \tag{29}$$

$$K_p = \frac{0.9 \times T}{L} \tag{30}$$

$$K_i = \frac{K_p}{T_i} \tag{31}$$

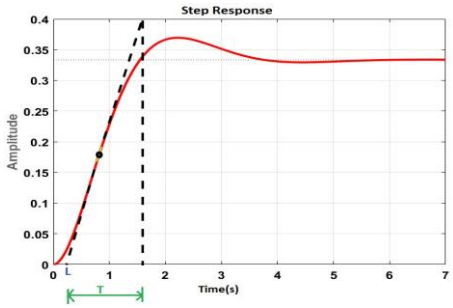

Fig -16: Zeigler Nichol's Optimisation

From Eq.(29)-(31), the controller parameters can be calculated as, K_P = 25.5; K_i = 63.6.

In this paper more emphasis is given to improving the dynamic response of the boost converter by identifying the best values for the controller parameters. The dynamic parameters considered in this paper are rise time (tr), settling time (ts), peak time(tp), peak overshoot(Mp), and delay time(td).

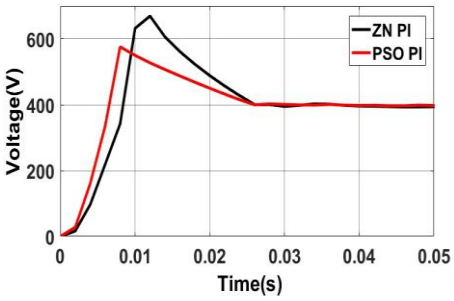

Fig -17: Zeigler Nichol's And PSO Comparison

Same input from the fuel cell source is given and output voltages with PSO and Zeigler Nichol's Optimisation are shown in Fig.17. The output voltage response with PSO has better response as compared to that with ZN . Peak overshoot is reduced from 0.7% to 0.45%. Faster response is obtained by reducing settling time, delay time and rise time. Also the output voltage ripple is reduced. Table 3. shows the performance comparison of ZN and PSO based PI controller. Thus the overall static and dynamic performance of the system is improved with Particle Swarm Optimization.

Table -3: Performance Comparison

Parameter	ZN-PI Controller	PSO-PI Controller
Peak Overshoot (%)	0.7	0.45
Settling time(s)	0.028	0.025
Delay Time(s)	0.006	0.004
Rise Time(s)	0.008	0.006

9. CONCLUSION

A high voltage gain DC-DC Boost converter with a wide input range, continuous input current and common ground points between the input side and the load side has been proposed in this paper. It is suitable for the power interface between a fuel cell source and the DC bus for the motor drive in fuel cell vehicles. The design of a closed loop continuous conduction mode operation converter with PSO Optimization technique can identify the controller parameters. The attributes of the large-signal model of the power converter, together with those of the optimization algorithm, provide excellent static and dynamic characteristics at all operating points.

REFERENCES

[1] Yun Zhang, Heyu Liu, Jing Li, Mark Sumner, and Changliang Xia, "A DC-DC Boost Converter with a Wide Input Range and High Voltage Gain for Fuel Cell Vehicles", IEEE Transactions On Power Electronics, Vol. 34, No. 5, 4100-4111p, May 2019.

[2] Haytham Abdelgawad and Vijay Sood, "Boost Converter Controller Design Based on Particle Swarm Optimization (PSO)," International Journal on Power Engineering and Energy (IJPEE), Vol. 7, No.2,April. 2016, 647-659p.

[3] Ching-Tsai Pan, Chen-Feng Chuang, and Chia-Chi Chu, "A Novel Transformer-less Adaptable Voltage Quadrupler DC Converter with Low Switch Voltage Stress", IEEE Transactions On Power Electronics, Vol. 29, No.9, 4787-4796p, Sept. 2014.

[4] Marcos Prudente, Luciano L. Pfitscher, Gustavo Emmendoerfer, Eduardo F. Romaneli, and Roger Gules, "Voltage Multiplier Cells Applied to Non-Isolated DC–DC Converters", IEEE Transactions On Power Electronics, Vol. 23, No.2, 871-887p, March.2008.

[5] G. Dotelli, R. Ferrero, P. G. Stampino, S. Latorrata, and S. Toscani, "PEM fuel cell drying and flooding diagnosis with signals injected by a power converter", IEEE Transactions On Instrumental Measurements, Vol. 64, No. 8, pp. 2064–2071, Aug. 2015.

[6] Q. Zhao, F. C. Lee, "High-efficiency high step-up dc–dc converters", IEEE Transactions On Power Electronics, Vol. 18, No. 1, pp. 65-73, Jan. 2003.

[7] F. L. Tofoli, D. de Castro Pereira, W. J. de Paula, and D. de Sousa Oliveira Junior, "Survey on non-isolated high-voltage step-up DC-DC topologies based on the boost converter", IET Power Electronics, Vol. 8, No. 10, pp. 2044–2057, 2015.

[8] J. H. Lee, T. J. Liang, and J. F. Chen, "Isolated coupled-inductor integrated DC-DC converter with nondissipative snubber for solar energy applications", IEEE Transactions On Industrial Electronics, Vol. 61, No. 7, pp. 3337–3348, Jul. 2014.

[9] W. H. Li, X. N. He, "Review of Nonisolated High-Step-Up DC/DC Converters in Photovoltaic Grid-Connected Applications", IEEE Transactions On Industrial Electronics, Vol. 58, No. 4, pp. 1239–1250, Apr. 2011.

[10] P. Sadat, and K. Abbaszadeh, "A Single-Switch High Step-Up DC–DC Converter Based on Quadratic Boost", IEEE Transactions On Industrial Electronics, Vol. 63, No.12, pp.2959-2968, Dec.2016.

[11] H. Choi, M. Ciobotaru, M. Jang, and V. G. Agelidis, "Performance of medium-voltage DC-bus PV system architecture utilizing high-gain DCDC converter", IEEE Transactions On Sustainable Energy, Vol. 6, No. 2, pp. 464–473, Apr. 2015.

[12] J. Leyva-Ramos, M. G. Ortiz-Lopez, L. H. Diaz-Saldierna, and J. A. Morales-Saldana, "Switching regulator using a quadratic boost converter for wide dc conversion ratios", IET Power Electronics, Vol. 2, No. 5, pp. 605–613, Sep. 2009.

[13] B. Axelrod, Y. Berkovich and A. Ioinovici, "Switched -capacitor/ switched-inductor structures for getting transformerless hybrid DC–DC PWM converters", IEEE Transactions On Circuits and Systems, Vol. 55, No. 2, pp. 687-696, Mar. 2008.

[14] A. Ioinovici, "Switched-capacitor power electronics circuits", IEEE Transactions On Circuits and System Magnetisation, Vol. 1, No. 4, pp. 37-42, Sep. 2001.

[15] G. Wu, X. Ruan, and Z. Ye, "Nonisolated high step-up dc-dc converters adopting switched-capacitor cell", IEEE Transactions On Industrial Electronics, Vol. 61, No. 1, pp. 383-393, Jan. 2015.

[16] Y. Tang, T. Wang, and Y. He, "A switched-capacitor-based activenetwork converter with high voltage gain",IEEE Transactions On Power Electronics, Vol. 29, No. 6, pp. 2959–2968, Jun. 2014.

[17] B. Axelrod, Y. Berkovich, and A. Ioinovici, "Transformerless DC-DC converters with a very high DC line-to-load voltage ratio", J. Circuits System Computations, Vol. 13, No. 3, pp. 467-475, Jun. 2004.

[18] Patidar, K., Umarikar, A.C., "High step-up pulse-width modulation dc–dc converter based on quasi-Z-source topology", IET Power Electronics, Vol. 8, No. 4, pp. 477–488, 2015.

[19] Y. Zhang, J. Shi, L. Zhou, J. Li, M. Sumner, P. Wang, and C. Xia, "Wide Input-Voltage Range Boost Three-Level DC-DC Converter with
Quasi-Z Source for Fuel Cell Vehicles", IEEE Transactions On Power Electronics Vol. 32, No. 9, pp. 6728–6738, Sep. 2017.

[20] G. Zhang, B. Zhang, Z. Li, D. Qiu, L. Yang, and W. A. Halang. "A 3-Znetwork boost converter", IEEE Transactions On Industrial Electronics, Vol. 62No. 1, pp. 278-288, Jan. 2015.